

Simultaneous sub-Doppler laser cooling of ${}^6\text{Li}$ and ${}^7\text{Li}$ isotopes

Gentle Dash, Tim de Jongh , Maxime Dixmieras , Christophe Salomon, and Tarik Yefsah *

Laboratoire Kastler Brossel, ENS-Université PSL, CNRS, Sorbonne Université, Collège de France, 24 rue Lhomond, 75005 Paris, France



(Received 8 June 2022; accepted 19 August 2022; published 12 September 2022)

We report on the simultaneous sub-Doppler laser cooling of ${}^6\text{Li}$ and ${}^7\text{Li}$ isotopes using gray molasses operating on their respective D_1 atomic transitions. For ${}^7\text{Li}$ we show that the sub-Doppler cooling can be achieved with two distinct Λ -type transitions, where the upper level can be either of the two $2^2P_{1/2}$ hyperfine states. We obtain temperatures of $\sim 85\ \mu\text{K}$, with atom numbers of $\sim 10^8$, and phase-space densities in the range of 10^{-6} – 10^{-5} for both isotopes. These conditions provide a good starting point for loading the mixture into an optical dipole trap and performing evaporative cooling to quantum degeneracy. Our work provides a valuable simplification for the preparation of ultracold ${}^6\text{Li}$ - ${}^7\text{Li}$ mixtures, which were proven to be a successful system for the study of impurity physics and Bose-Fermi superfluids.

DOI: [10.1103/PhysRevA.106.033105](https://doi.org/10.1103/PhysRevA.106.033105)

I. INTRODUCTION

The study of ultracold atomic mixtures offers the possibility to explore a wide scope of quantum phenomena ranging from few-body to many-body physics [1,2]. Such mixtures provide the starting point for a variety of systems, from immersed impurities [3–7] to Efimov states [8–10], ground-state molecules [11–14], and degenerate Bose-Fermi mixtures [15–18]. A prominent example in the field of many-body physics is the observation of dual Bose-Fermi superfluidity, which was achieved for the first time using an ultracold mixture of lithium-6 (${}^6\text{Li}$) and lithium-7 (${}^7\text{Li}$) isotopes [19], unlocking a new area of ultracold physics. Soon after, other Bose-Fermi superfluids were observed with mixtures of ${}^6\text{Li}$ - ${}^{41}\text{K}$ [20] and ${}^6\text{Li}$ - ${}^{174}\text{Yb}$ [21]. These experimental advances have intensified the interest in superfluid mixtures, triggering a renewed theoretical effort on the topic and raising a series of novel conceptual questions [22–26].

From the quantum simulation perspective, dual superfluid experiments represent promising platforms where interisotope or interspecies interactions can be tuned. Moreover, the available realizations of such mixtures allow exploration of the role of the mass difference between the bosonic and fermionic particles, ranging from weak mass imbalance for ${}^6\text{Li}$ - ${}^7\text{Li}$, to intermediate for ${}^6\text{Li}$ - ${}^{41}\text{K}$, to extreme for ${}^6\text{Li}$ - ${}^{174}\text{Yb}$. However, in practice, the benefits of such platforms are limited by the significant technical overhead in development and maintenance. Even in the case of ${}^6\text{Li}$ - ${}^7\text{Li}$, which is technologically the simplest owing to the ability to use solid-state diode lasers at 671 nm for both isotopes, the preparation of an ultracold mixture has historically been tedious. The difficulty with the existing approach for ${}^6\text{Li}$ - ${}^7\text{Li}$ [7,19,27] resides in bringing the temperature of the mixture from the millikelvin range, typically achieved in magneto-optical traps, to the $\lesssim 100\ \mu\text{K}$ range necessary to load the mixture in an optical dipole trap

of reasonable power, where evaporative cooling to quantum degeneracy and double superfluidity can be performed.

Here, we propose a significant simplification of this critical stage by demonstrating the simultaneous sub-Doppler cooling of ${}^6\text{Li}$ and ${}^7\text{Li}$. The method is based on gray-molasses cooling operating on the respective D_1 atomic transitions ($2^2S_{1/2} \rightarrow 2^2P_{1/2}$) of the two isotopes. While D_1 gray-molasses cooling was already achieved for ${}^7\text{Li}$ [28] and ${}^6\text{Li}$ [29] independently, the feasibility of their simultaneous operation is not evident given the proximity of the D_1 transition of ${}^7\text{Li}$ to the D_2 transition ($2^2S_{1/2} \rightarrow 2^2P_{3/2}$) of ${}^6\text{Li}$, as illustrated in Fig. 1. In this work, we explore this simultaneous cooling for two distinct Λ -type transitions of ${}^7\text{Li}$ by using either of the two hyperfine levels $|2^2P_{1/2}, F_e = 1\rangle$ and $|2^2P_{1/2}, F_e = 2\rangle$ as the excited state, with F_e being the hyperfine angular momentum quantum number of the upper electronic state.

When the D_1 cooling of ${}^7\text{Li}$ is performed via the $|2^2P_{1/2}, F_e = 2\rangle$ hyperfine level, such that the proximity of the transitions is best evaded, we obtain efficient simultaneous cooling of both isotopes to temperatures $\lesssim 100\ \mu\text{K}$ on a millisecond timescale. We find that the main adverse effect of the ${}^7\text{Li}$ cooling light on the ${}^6\text{Li}$ atoms is a reduced molasses lifetime to a few tens of milliseconds, which is, nonetheless, much larger than the timescale needed for the molasses to reach its equilibrium temperature ($\sim 1\ \text{ms}$) and to subsequently load the mixture into a dipole trap. On the contrary, when the D_1 cooling of ${}^7\text{Li}$ is performed via the $|2^2P_{1/2}, F_e = 1\rangle$ hyperfine level, we observe rapid destruction of the ${}^6\text{Li}$ cloud due to the near coincidence between the ${}^7\text{Li}$ cooling beam's frequency and the D_2 transition frequency for ${}^6\text{Li}$. We circumvent this detrimental effect by applying an alternating pulse sequence of the molasses beams and achieve concurrent cooling to temperatures $\lesssim 100\ \mu\text{K}$ for both isotopes.

In both cases we thus reach the desired temperature range. The achieved phase-space densities (PSDs) are on the order of 10^{-6} – 10^{-5} , offering a good starting point for loading the atoms into an optical dipole trap and evaporatively cooling

*Corresponding author: tarik.yefsah@lkb.ens.fr

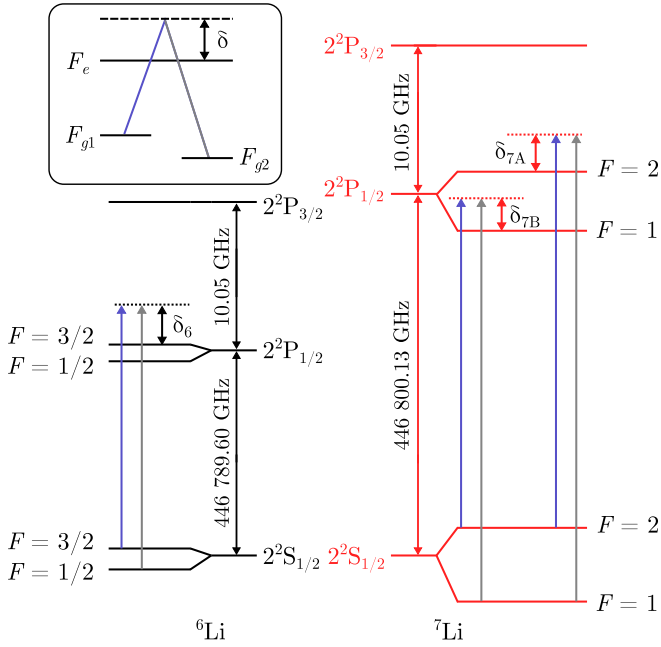


FIG. 1. Energy-level scheme showing the D_1 transitions for the ${}^6\text{Li}$ and ${}^7\text{Li}$ isotopes. The upper electronic state involved in the D_2 transition is also shown. The blue and gray arrows indicate the two frequencies of the D_1 gray-molasses cooling beams, which we refer to as the strong and weak arms, respectively, due to their relative laser intensity. The one-photon detuning for the ${}^6\text{Li}$ molasses is indicated by δ_6 , while the one-photon detuning for the ${}^7\text{Li}$ molasses is indicated by δ_{7A} (δ_{7B}) for the configuration with $F_e = 2$ ($F_e = 1$) as the upper state. The Raman condition is ensured for all transitions. These laser-cooling configurations can be represented by a Λ scheme, as displayed in the inset, with one-photon detuning δ . See the text for details on the addressed transitions.

the mixture to quantum degeneracy. This work shows that this simultaneous gray-molasses cooling method is robust and provides a substantial simplification for the preparation of superfluid Bose-Fermi mixtures of ${}^6\text{Li}$ and ${}^7\text{Li}$.

II. EXPERIMENTAL PROTOCOL

A. Overview

Our experiment starts with a dual magneto-optical trap (MOT) of ${}^6\text{Li}$ and ${}^7\text{Li}$ inside a glass cell, loaded from a Zeeman-slowed atomic beam of lithium enriched in ${}^6\text{Li}$. After loading the MOT for typically 8 s, we apply a simple compression stage (CMOT) in which the laser detunings are reduced. We subsequently turn off the magnetic quadrupole field while keeping the MOT laser beams on for 0.5 ms to hold the atoms until all transient magnetic fields have fully decayed ($\sim 250 \mu\text{s}$) and only residual static magnetic fields remain. We will refer to this stage as the D_2 optical molasses phase, although transient magnetic gradients are still present for the first half of this phase. In the last stage of the preparation sequence, we switch off all the MOT beams and turn on the D_1 laser-cooling beams for 1.5 to 3 ms to create gray molasses.

D_1 gray molasses is a bichromatic laser-cooling technique that applies to atoms with a well-resolved Λ -type three-level structure, typically connecting two nondegenerate hyperfine

ground states F_{g1} and F_{g2} to an upper state F_e via strong- and weak-coupling lasers, respectively [28]. This is shown schematically in Fig. 1. Each frequency component is blue detuned with respect to either the $F_{g1} \rightarrow F_e$ or $F_{g2} \rightarrow F_e$ transition. In such molasses, two mechanisms—both involving dark states—work in tandem to provide sub-Doppler cooling of the atoms: Sisyphus-like cooling on a $F_{g1} \rightarrow F_e$ transition with either $F_e = F_{g1}$ or $F_e = F_{g1} - 1$ [30–32] and a two-photon effect similar to velocity-selective coherent population trapping via a (coherent) Raman process connecting the two hyperfine ground states according to the Λ structure [28]. This cooling method has been successfully applied to and proven to be efficient for several alkali atoms such as ${}^6\text{Li}$ [29,33], ${}^7\text{Li}$ [28,34], ${}^{23}\text{Na}$ [35], ${}^{39}\text{K}$ [36,37], ${}^{40}\text{K}$ [38], ${}^{41}\text{K}$ [39], and ${}^{87}\text{Rb}$ [40].

For ${}^6\text{Li}$, we use the $F_{g1} = 3/2 \rightarrow F_e = 3/2$ and $F_{g2} = 1/2 \rightarrow F_e = 3/2$ transitions of the D_1 line. Gray-molasses cooling could, in principle, also be applied using the $F_e = 1/2$ state, but the small hyperfine splitting within the $2^2P_{1/2}$ electronic state of 26 MHz $\sim 4\Gamma$, with $\Gamma = 2\pi \times 5.87$ MHz being the excited state linewidth, is not sufficient to prevent competing effects between the two hyperfine levels. For ${}^7\text{Li}$, the hyperfine splitting is sufficient that we can explore the two possible Λ schemes on the D_1 transition: (i) $F_{g1} = 2 \rightarrow F_e = 2$ and $F_{g2} = 1 \rightarrow F_e = 2$ and (ii) $F_{g1} = 2 \rightarrow F_e = 1$ and $F_{g2} = 1 \rightarrow F_e = 1$.

The energy-level diagram in Fig. 1 shows the D_1 and D_2 lines of the ${}^6\text{Li}$ and ${}^7\text{Li}$ isotopes, which are the four lines relevant to the present work. In the following we will refer to these four lines as L_{16} , L_{26} , L_{17} , and L_{27} , with the first digit of the subscript referring to the electronic transition (D_1 or D_2) and the second digit referring to the mass of the isotope, and we will use a superscript of the form $F_g \rightarrow F_e$ to specify the hyperfine transition when needed. Table I displays the frequency difference among various hyperfine transitions among these lines, where we note a close proximity of the $L_{26}^{1/2 \rightarrow 1/2}$ and $L_{26}^{1/2 \rightarrow 3/2}$ transitions of ${}^6\text{Li}$ with $L_{17}^{2 \rightarrow 1}$, on the one hand ($\sim 5\Gamma$), and with $L_{17}^{2 \rightarrow 2}$, on the other hand ($\sim 10\Gamma$). Note that the situation is particularly problematic in the former case, as the strong D_1 cooling beam of ${}^7\text{Li}$ is required to be typically 3Γ – 5Γ blue detuned from $L_{17}^{2 \rightarrow 1}$. This proximity raises the question of whether it is possible to perform D_1 cooling on ${}^7\text{Li}$ without altering the ${}^6\text{Li}$ cloud. This issue is addressed throughout this paper.

B. Laser setup

All laser beams are derived from four distinct extended-cavity diode lasers at 671 nm, each being independently frequency locked on the relevant lines (two of them on L_{16} , one on L_{17} , and one on L_{27}). Each laser provides about 20 mW of laser power, which undergoes a single or multiple amplification stages via injection of tapered amplifiers or seeding of high-power diodes through injection locking, providing sufficient power at all required frequencies for Zeeman slowing, laser cooling, and imaging.

For each isotope, the MOT operates with two frequencies: one cooling frequency and one repumper frequency. The cooling beam is red detuned by 4.4Γ (3.9Γ) from the transition $L_{26}^{3/2 \rightarrow 5/2}$ for ${}^6\text{Li}$ ($L_{27}^{2 \rightarrow 3}$ for ${}^7\text{Li}$). The MOT repumper

TABLE I. Hyperfine transitions of the D_1 and D_2 lines of both lithium isotopes. Frequencies are taken from [41]. The rightmost column gives the frequency difference $\Delta\nu$ between each transition and the $L_{17}^{2\rightarrow 1}$ transition.

	Transition $F_g \rightarrow F_e$	Label	Frequency ν (MHz)	$\Delta\nu$ (MHz)
${}^6\text{Li}$ D_2 line (L_{26})	$3/2 \rightarrow 5/2$	$L_{26}^{3/2\rightarrow 5/2}$	446 799 571	-200 (-34.1 Γ)
	$3/2 \rightarrow 3/2$	$L_{26}^{3/2\rightarrow 3/2}$	446 799 574	-197 (-33.6 Γ)
	$3/2 \rightarrow 1/2$	$L_{26}^{3/2\rightarrow 1/2}$	446 799 576	-195 (-33.3 Γ)
	$1/2 \rightarrow 3/2$	$L_{26}^{1/2\rightarrow 3/2}$	446 799 802	31.1 (5.3 Γ)
	$1/2 \rightarrow 1/2$	$L_{26}^{1/2\rightarrow 1/2}$	446 799 804	32.8 (5.6 Γ)
${}^7\text{Li}$ D_1 line (L_{17})	$2 \rightarrow 1$	$L_{17}^{2\rightarrow 1}$	446 799 771	
	$2 \rightarrow 2$	$L_{17}^{2\rightarrow 2}$	446 799 863	91.9 (15.6 Γ)
	$1 \rightarrow 1$	$L_{17}^{1\rightarrow 1}$	446 800 575	803 (137 Γ)
	$1 \rightarrow 2$	$L_{17}^{1\rightarrow 2}$	446 800 666	895 (152 Γ)

frequency is red detuned by 2.9Γ (2.2Γ) from the transition $L_{16}^{1/2\rightarrow 1/2}$ for ${}^6\text{Li}$ ($L_{27}^{1\rightarrow 2}$ for ${}^7\text{Li}$). Note here that the ${}^6\text{Li}$ MOT repumper operates near the D_1 line instead of D_2 in order to avoid losses of ${}^7\text{Li}$ due to the vicinity of L_{26} and L_{17} [42]. Four laser beams, each at one of these four frequencies, are generated and spatially superimposed to follow the same optical path where they are each split into six independent beams to create pairs of σ^+ - σ^- counterpropagating beams along three orthogonal directions. The same 24 beams are used for the CMOT and D_2 molasses phases, where their frequencies are shifted (typically by a few Γ) to optimal detunings.

For the gray molasses we use laser beams with two frequency components, which we obtain by generating a low-amplitude (approximately 8%) sideband via an electro-optic modulator. This ensures phase coherence of the (high-amplitude) carrier and (low-amplitude) sideband, which is essential to obtain Λ enhancement of the gray-molasses cooling [28,40]. For each isotope the sideband is generated at a frequency corresponding to the hyperfine splitting of the ground states: +228 MHz (+803.5 MHz) for ${}^6\text{Li}$ (${}^7\text{Li}$). The laser frequencies are blue detuned from the relevant D_1 transitions as depicted in Fig. 1.

For ${}^6\text{Li}$, the strong (weak) amplitude component of the molasses beams is blue detuned by $\delta_6 = 5.2\Gamma$ from $L_{16}^{3/2\rightarrow 3/2}$ ($L_{16}^{1/2\rightarrow 3/2}$). For ${}^7\text{Li}$, as indicated, we investigate two possible Λ schemes: configuration A, where we use $|2^2 P_{1/2}, F_e = 2\rangle$ as the upper state, and configuration B, for which the upper state is $|2^2 P_{1/2}, F_e = 1\rangle$. In configuration A, the detuning of the strong (weak) amplitude component from $L_{17}^{2\rightarrow 2}$ ($L_{17}^{1\rightarrow 2}$) is denoted by δ_{7A} . We study the effects of δ_{7A} on both the ${}^7\text{Li}$ and ${}^6\text{Li}$ atoms in order to assess whether the proximity between L_{26} and L_{17} is detrimental to the simultaneous cooling. In configuration B, the strong (weak) amplitude component of the molasses beams is detuned from $L_{17}^{2\rightarrow 1}$ ($L_{17}^{1\rightarrow 1}$) by $\delta_{7B} = 2.5\Gamma$. This value of δ_{7B} sets the two frequencies at over 10Γ red detuned from the transitions involving the $|2^2 P_{1/2}, F_e = 2\rangle$ state of ${}^7\text{Li}$, making the off-resonant scattering due to this level negligible.

The D_1 cooling beams follow the same optical path as the MOT beams and form three pairs of counterpropagating beams in a σ^+ - σ^- configuration. At the science cell, each of the six resulting gray-molasses beams has a power of 9.0

and 4.5 mW and a waist ($1/e^2$ width) of approximately 3 and 2 mm for ${}^6\text{Li}$ and ${}^7\text{Li}$, respectively, resulting in peak intensities in the range of $I \approx 3I_{\text{sat}} - 6I_{\text{sat}}$ and $I \approx 7I_{\text{sat}} - 11I_{\text{sat}}$, with $I_{\text{sat}} = 7.6 \text{ mW/cm}^2$ being the saturation intensity for the D_1 transition.

C. Detection

Following the gray-molasses stage, we switch off all laser beams and let the atoms expand freely. After a certain time of flight (TOF) we detect the atoms through low-saturation absorption imaging using a $10\text{-}\mu\text{s}$ pulse of circularly polarized probe beams that are resonant with the respective D_2 lines $L_{26}^{3/2\rightarrow 5/2}$ and $L_{27}^{2\rightarrow 3}$. For each isotope, we shine a repumper beam (tuned to $L_{27}^{1/2\rightarrow 3/2}$ and $L_{27}^{1\rightarrow 2}$) for $10\text{ }\mu\text{s}$ before imaging in order to transfer all atoms to the upper hyperfine ground state ($F_g = 3/2$ for ${}^6\text{Li}$ and $F_g = 2$ for ${}^7\text{Li}$), and then during the imaging phase, we apply a second repumping pulse to compensate for pumping effects into the lower hyperfine ground states. These repumping beams are directed along the two axes perpendicular to the imaging direction. The absorption shadow of the atoms is then collected by a CCD camera and converted to an optical density profile.

We convert the optical densities into atomic densities using absorption cross sections of $0.59\sigma_0$ and $0.48\sigma_0$ for ${}^6\text{Li}$ and ${}^7\text{Li}$, respectively, where $\sigma_0 = \frac{3\lambda^2}{2\pi}$, with λ being the wavelength of the resonant imaging light. These values correspond to the theoretical values computed at zero magnetic field by assuming that for each isotope all atoms occupy the upper hyperfine ground state ($F_g = 3/2$ for ${}^6\text{Li}$ and $F_g = 2$ for ${}^7\text{Li}$) with equal populations in the m_F levels, with m_F being the quantum number associated with projection of the hyperfine angular momentum onto a quantization axis. In practice, the magnetic field is nonzero, and we measured it to be 0.4(2) G using ${}^7\text{Li}$ hyperfine absorption spectra as a magnetometer, yielding a reduction in the absorption cross sections stated above by about 5% and 10%, respectively, according to our calculations. For simplicity, we will, however, deliberately ignore this reduction, which implies that the atom numbers stated throughout the paper are slightly underestimated.

The resulting atomic density profiles are fitted with a two-dimensional Gaussian function yielding peak density n_0 ,

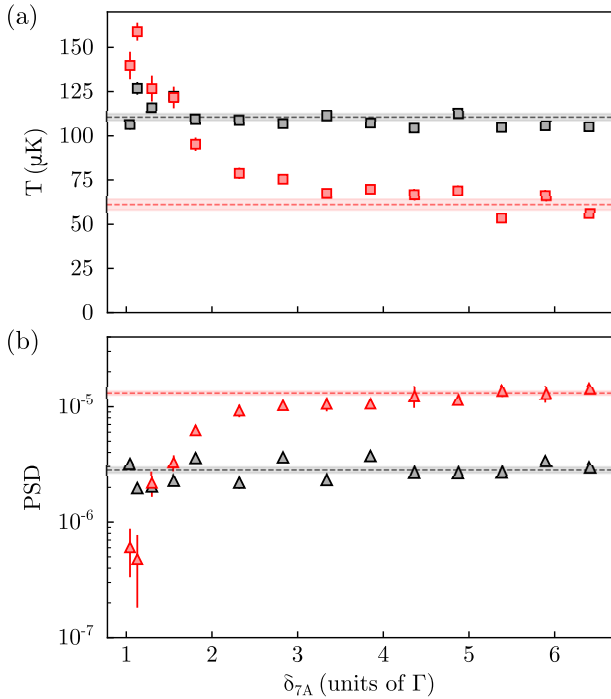


FIG. 2. (a) Temperatures and (b) PSDs of the clouds after 1.5 ms of simultaneous gray-molasses cooling in configuration A as a function of δ_{7A} . Black (red) data points correspond to values of ^6Li (^7Li). Error bars represent statistical uncertainties at one standard deviation determined with the bootstrap method [43]. Dashed lines show average temperatures and phase-space densities for the respective isotopes for $\delta_{7A} > 4\Gamma$, and the shaded regions indicate the corresponding standard error.

atom number, and cloud sizes. By varying the TOF we determine the ballistic expansion rate of the atoms and extract temperatures T of the clouds. Finally, we determine the peak PSD $n_0 \Lambda_T^3$, where $\Lambda_T = \frac{h}{\sqrt{2\pi m k_B T}}$ is the thermal de Broglie wavelength. Note that the uncertainty of the imaging system magnification was measured to be 2.3%, resulting in systematic relative errors of 4.6% and 9.2%, respectively, for temperatures and PSDs reported in this paper.

III. RESULTS

When loading the MOT for 8 s, we routinely capture $9(1) \times 10^7$ ^6Li atoms and $13(2) \times 10^7$ ^7Li atoms in the D_2 molasses and obtain temperatures of approximately 0.7 mK for both isotopes. All atoms present at the D_2 stage are captured in the gray molasses. Optimization and characterization of the gray molasses for each cooling configuration are discussed below.

A. Cooling on the $F_e = 2$ state of ^7Li

In configuration A, where ^7Li is cooled via the $F_e = 2$ upper state, the ^7Li transition is 10Γ blue detuned from the $L_{26}^{1/2 \rightarrow 1/2, 3/2}$ lines of ^6Li . Additional blue detuning of the ^7Li gray-molasses beams (given by δ_{7A}) moves the cooling lasers further away from the ^6Li resonance. In Fig. 2, we report ^6Li and ^7Li temperatures for 1.5-ms simultaneous gray-molasses

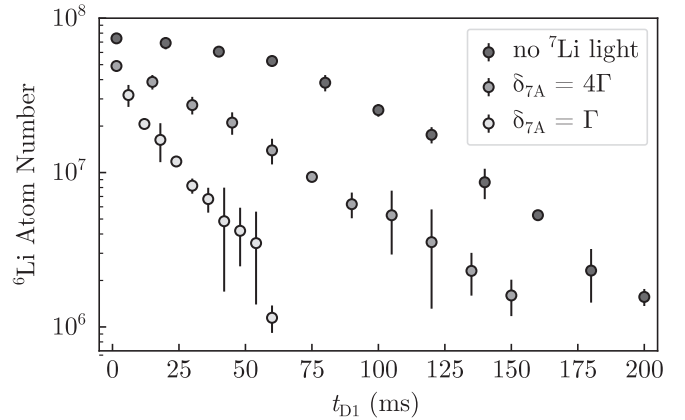


FIG. 3. Semilogarithmic plot of the ^6Li atom number as a function of D_1 molasses duration t_{D1} for three distinct situations: in the absence of ^7Li molasses light (dark gray circles), in the presence of ^7Li molasses light with $\delta_{7A} = 4\Gamma$ (medium gray circles), and in the presence of ^7Li molasses light with $\delta_{7A} = \Gamma$ (light gray circles). Error bars represent statistical uncertainties at one standard deviation.

cooling at several values of δ_{7A} while maintaining the respective Raman conditions.

We observe that the ^7Li gray-molasses cooling is efficient for a broad range of one-photon detunings, becoming less effective only for $\delta_{7A} < 3\Gamma$, and that for this entire range the influence of the ^7Li cooling light on the ^6Li temperatures and atom numbers is negligible. We readily obtain temperatures of $T_6 = 105(2) \mu\text{K}$ and $T_7 = 56(2) \mu\text{K}$ and phase-space densities of $3.0(1) \times 10^{-6}$ and $1.4(1) \times 10^{-5}$ for ^6Li and ^7Li , respectively, which are well within the range of parameters for efficient loading into a dipole trap, although the factor of 2 between T_6 and T_7 could be unpractical. Upon intensity ramp of the D_1 molasses laser beams, we were able to obtain a better compromise, with $T_6 = 90(3) \mu\text{K}$ and $T_7 = 83(3) \mu\text{K}$, leading to phase-space densities of $3.1(2) \times 10^{-6}$ and $9.0(7) \times 10^{-6}$, respectively. These ^6Li temperatures are slightly higher than reported in previous experiments [19,29,33,44], which we ascribe to imperfect magnetic field cancellation in our setup where the residual magnetic field is ~ 0.4 G. Nonetheless, this simultaneous cooling method still provides a good starting point for loading the cloud into a dipole trap and initiating evaporation.

While the ^6Li clouds are hardly affected by the ^7Li cooling beams for D_1 molasses durations of a few milliseconds, we observe a marked effect at longer times, which is revealed in the lifetime of the ^6Li atoms in the molasses. Figure 3 displays the number of ^6Li atoms as a function of hold time in the molasses in the absence and in the presence of ^7Li molasses light for two distinct values of δ_{7A} . We observe a faster decay of the atom number in the presence of ^7Li molasses light that gets stronger as the ^7Li cooling light frequency is shifted towards the ^6Li resonance, as is expected from the enhanced photon scattering rate. Overall, the main adverse effect of the ^7Li cooling light on the ^6Li atoms is thus a reduced molasses lifetime from ~ 150 ms to a few tens of milliseconds. This relatively short lifetime is, nonetheless, much larger than the timescale needed for the molasses to reach its equilibrium

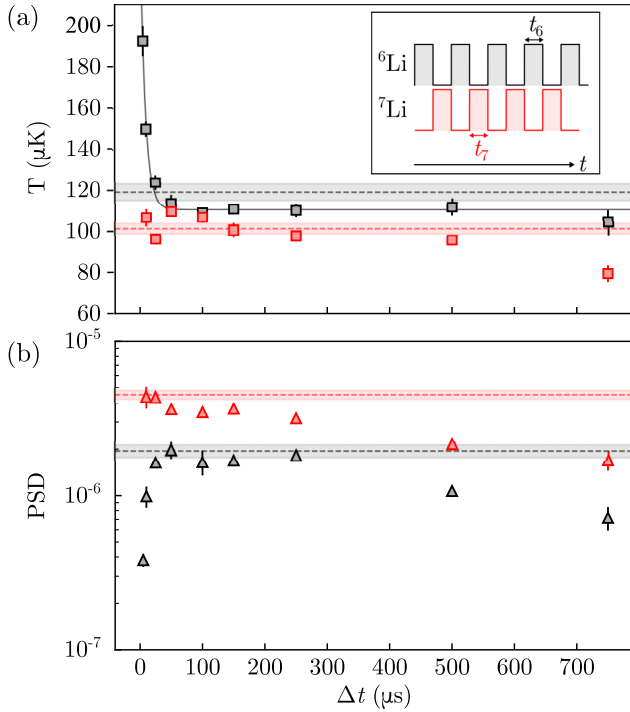


FIG. 4. Optimization of the individual pulse duration for gray-molasses cooling in the alternating cooling sequence of configuration B. Black (red) data points correspond to values of ${}^6\text{Li}$ (${}^7\text{Li}$). (a) Temperatures after 3 ms of pulsed gray-molasses cooling. Dashed lines show temperatures obtained when cooling each isotope individually with a continuous pulse of 1.5 ms, with the shaded areas indicating the statistical error at one standard deviation. The solid gray line shows an exponential fit of the ${}^6\text{Li}$ temperatures to guide the eye. The inset shows a schematic representation of the pulse sequence. (b) PSDs for ${}^6\text{Li}$ and ${}^7\text{Li}$. Dashed lines represent PSDs for individual cooling.

temperature (~ 1 ms) and to subsequently load the mixture into a dipole trap.

B. Cooling on the $F_e = 1$ state of ${}^7\text{Li}$

In configuration B, where cooling of ${}^7\text{Li}$ is performed via the $F_e = 1$ upper state, the spectral-line proximity does hinder the simultaneous cooling of the two isotopes: At $\delta_{7B} = 2.5\Gamma$ the ${}^7\text{Li}$ cooling beam that acts on the $L_{17}^{2 \rightarrow 1}$ transition is only 3Γ red detuned from the $L_{26}^{1/2 \rightarrow 1/2, 3/2}$ lines. At such a detuning the ${}^7\text{Li}$ light is expected to considerably heat up the ${}^6\text{Li}$ cloud, which we confirmed experimentally. Moreover, we observe that simultaneous operation of both molasses leads to stronger detrimental effects with a rapid destruction of the ${}^6\text{Li}$ cloud (see Sec. IV). To circumvent this, we employ a temporally alternating pulse sequence by shining the ${}^6\text{Li}$ and ${}^7\text{Li}$ molasses in successive pulses (see the inset in Fig. 4). This technique is very similar to earlier work on atom tweezers [45], single-atom imaging of ${}^6\text{Li}$ [46], and molecule experiments [47–49], in which adverse effects of laser light are circumvented via periodic amplitude modulation. Here, we aim to find an optimal pulsed scheme in which we alternate between cooling and heating cycles on the ${}^6\text{Li}$ atoms such

that the heating due to the ${}^7\text{Li}$ molasses beams is largely compensated by the cooling power of the ${}^6\text{Li}$ molasses. This additionally prevents the rapid destruction of the ${}^6\text{Li}$ cloud observed when simultaneously operating both molasses.

We therefore employ a pulse sequence for which the ${}^6\text{Li}$ and ${}^7\text{Li}$ molasses beams are exactly out of phase. We refer to t_6 and t_7 as the pulse durations of ${}^6\text{Li}$ and ${}^7\text{Li}$, respectively. The pulsed sequence always starts with a ${}^6\text{Li}$ light pulse but can end with either a ${}^6\text{Li}$ or ${}^7\text{Li}$ light pulse. Typically, the total D_1 gray-molasses duration is 3 ms to obtain effective cooling periods similar to those in configuration A (~ 1.5 -ms molasses time). In order to optimize the pulse sequence we first explore the situation where $t_6 = t_7 = \Delta t$, with a final pulse of ${}^6\text{Li}$ light. The results are shown in Fig. 4, where we observe that for $\Delta t \gtrsim 50 \mu\text{s}$ we obtain temperatures $\lesssim 100 \mu\text{K}$, which are comparable to those obtained for separate cooling of each isotope with continuous molasses of 1.5 ms. The cooling of ${}^6\text{Li}$ atoms, however, is seen to be less efficient at smaller values of Δt . From this we infer that at these shorter pulse widths the ${}^6\text{Li}$ molasses is not able to compensate for the heating induced by the ${}^7\text{Li}$ beams. Note that we restricted the pulse duration to $\Delta t \leq 750 \mu\text{s}$ in order to limit the free expansion of the cloud when the cooling light is off. Indeed, the characteristic velocity of atoms at $100 \mu\text{K}$ is approximately 0.37 m/s, yielding a size of 0.37 mm after a free expansion of 1 ms, which should be compared to the initial size of the molasses clouds of $\lesssim 1$ mm and the laser beam waists of ~ 2 – 3 mm.

In order to improve further the performances of the pulsed scheme we varied a number of parameters. First, we investigated the role of the duty cycle by fixing t_6 to $100 \mu\text{s}$ while varying t_7 from 25 to $200 \mu\text{s}$, which did not show any influence on the final temperatures. Second, we also explored the situation where the pulse sequence ends on ${}^7\text{Li}$ light, which we found to yield systematically higher temperatures and lower PSDs (see below), as expected from the proximity of the $L_{17}^{2 \rightarrow 1}$ and $L_{26}^{1/2 \rightarrow 1/2, 3/2}$ lines. Finally, we implemented diverse schemes of intensity ramp down, which we found to yield the best results. In Fig. 5 we present an overview of three different pulse sequences (I, II, and III). In sequence I, we use $t_6 = t_7 = \Delta t = 100 \mu\text{s}$ and end on a ${}^7\text{Li}$ light pulse. In sequence II, we use $t_6 = 100 \mu\text{s}$ and $t_7 = 50 \mu\text{s}$ while ending on a ${}^6\text{Li}$ light pulse. Finally, sequence III corresponds to ramped pulse sequences (ending on ${}^6\text{Li}$ light) in which intensities are reduced by half over the total molasses duration of 3 ms.

The results summarized in Fig. 5 show that it is most favorable to combine ending the sequence on a pulse of ${}^6\text{Li}$ light together with an intensity ramp, yielding PSDs on the order of $\sim 4 \times 10^{-6}$ and temperatures of approximately $85 \mu\text{K}$ for both isotopes. These temperature and PSD values are obtained at the cost of a reduction in the atom numbers by only 18% (16%) for ${}^6\text{Li}$ (${}^7\text{Li}$). With this optimized pulsed scheme we are thus able to not only circumvent destruction of the ${}^6\text{Li}$ cloud due to the near-resonant light of the ${}^7\text{Li}$ molasses beams but also reach PSDs which are suitable for loading the atoms into an optical dipole trap but lower than PSDs obtained in configuration A for ${}^7\text{Li}$.

To understand the effect of the ${}^7\text{Li}$ molasses light on the ${}^6\text{Li}$ atoms, we repeat the temperature measurements in Fig. 4, altering the sequence by adding a final pulse of ${}^7\text{Li}$ light of

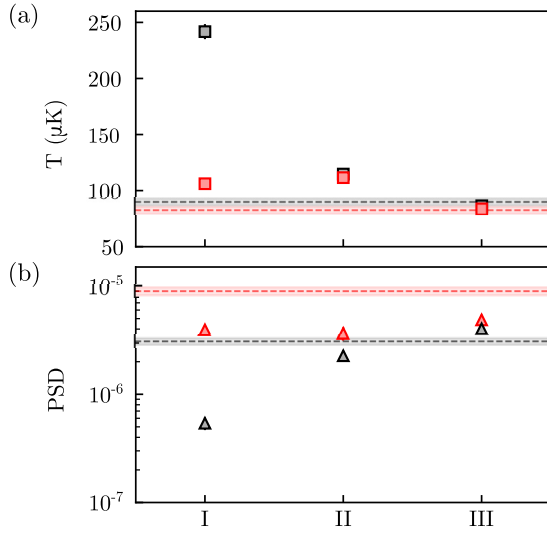


FIG. 5. (a) Temperatures and (b) phase-space densities for different pulse sequences employed for the alternating cooling of ^6Li (black) and ^7Li (red) for the configuration in which ^7Li is cooled via the $F_e = 1$ state with $\delta_{7B} = 2.5\Gamma$. Sequences ending on a ^7Li light pulse (I) lead to higher temperatures of the ^6Li cloud compared to a sequence ending on a ^6Li light pulse (II). For a ramped sequence (III) higher PSDs are obtained for both isotopes. See text for details on the sequences. Dashed lines represent the optimal temperatures and phase-space densities reached in configuration A, as shown in Fig. 2. Shaded areas correspond to the statistical error at one standard deviation.

width Δt , deliberately heating the ^6Li cloud. Figure 6 shows the obtained temperatures. First, we observe the occurrence of an optimum at $\Delta t \sim 50 \mu\text{s}$ with a ^6Li temperature of $\approx 180 \mu\text{K}$ that is substantially higher than the lowest temperatures reported above.

At short pulse duration, the ^6Li laser pulse cannot compensate the heating induced by the ^7Li light, similar to what was observed in Fig. 4. For longer pulse durations ($\Delta t \geq 50 \mu\text{s}$) we observe a linear increase of temperature, signaling a heating mechanism with a steady heating rate of $0.82(4) \text{ K/s}$. This heating can be explained by analyzing the photon scattering of ^6Li atoms exposed to ^7Li molasses light. The coupling of the carrier ^7Li molasses light to the ^6Li atoms via the $L_{26}^{1/2 \rightarrow 1/2, 3/2}$ and $L_{26}^{3/2 \rightarrow 1/2, 3/2, 5/2}$ transitions yields successive photon scattering cycles with two characteristic scattering rates of $\approx \Gamma/5$ and $\approx \Gamma/400$, respectively. Taking into account the combined effect of these photon scattering processes, we quantify the resulting momentum diffusion and obtain a heating rate of $\sim 0.9 \text{ K/s}$, in agreement with the measured value.

IV. DISCUSSION

In addition to the heating observed in Fig. 6, there are two other detrimental effects one may consider as a result of the proximity of the ^7Li molasses light to the L_{26} transitions: light shifts and net radiation pressure forces resulting from an imperfect intensity balance of the molasses beams. Light shifts induced by the ^7Li beams can, indeed, alter the Raman condition for the Λ scheme of the ^6Li molasses. However,

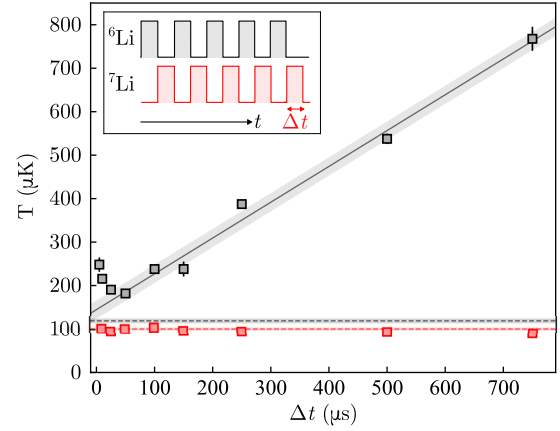


FIG. 6. Heating effects of the ^7Li gray-molasses cooling light on the ^6Li atoms. The same pulse sequences are used as for the data in Fig. 4, but a final pulse of ^7Li cooling light is added. Black (red) data points correspond to temperatures for ^6Li (^7Li). The dashed lines represent temperatures obtained for individual cooling of each isotope using a continuous 1.5-ms pulse, with the surrounding shaded areas indicating the statistical error at one standard deviation. The solid gray line represents a linear fit of the ^6Li temperatures taken for $\Delta t \geq 50 \mu\text{s}$, yielding a heating rate of $0.82(4) \text{ K/s}$. The inset shows a schematic representation of the pulse sequence.

we estimate these light shifts to be only on the order of $\hbar\Gamma$ and negative, such that the resulting change in the Raman condition merely leads to less efficient cooling; it would still allow us to reach temperatures of $\sim 100 \mu\text{K}$, as observed in previous studies [28,29,44]. Furthermore, the light shifts cannot account for the fact that, when both ^6Li and ^7Li act on the ^6Li cloud, the latter is rapidly expelled with an overall center-of-mass velocity of 10 times the recoil velocity.

On the other hand, a net radiation pressure resulting from an intensity imbalance among the molasses beams can have an important effect. Indeed, for scattering rates on the order of those discussed in Sec. III B, one would expect extremely high radiation pressure forces in the case of a cycling transition. When only the ^7Li light acts on the ^6Li cloud, this effect is transient and not dominant due to the noncycling nature of the $L_{26}^{1/2 \rightarrow 1/2, 3/2}$ and $L_{26}^{3/2 \rightarrow 1/2, 3/2, 5/2}$ transitions. However, when the ^6Li and ^7Li molasses beams are shone simultaneously, the effect of an intensity imbalance becomes dominant. In this case the strong ^6Li molasses light plays the role of a repumper for the $L_{26}^{1/2 \rightarrow 1/2, 3/2}$ transitions, making them effectively cycling with a scattering rate that we estimate to be $\approx \Gamma/10$. For such a high scattering rate, an intensity imbalance of only 1% would lead the atoms to experience an acceleration of 3 km/s^2 , which can, indeed, explain our observations. The pulsed scheme employed in configuration B therefore not only serves to alternate between cooling and heating cycles on the ^6Li atoms; it also prevents the large radiation pressure which causes the observed rapid destruction of the ^6Li cloud.

V. CONCLUSION

In this work we have demonstrated simultaneous D_1 gray-molasses cooling of ${}^6\text{Li}$ and ${}^7\text{Li}$. Two possible cooling configurations were explored. In the first configuration, in which we cool ${}^7\text{Li}$ via the upper hyperfine state ($F_e = 2$) of the $2^2 P_{1/2}$ level, simultaneous cooling is straightforward and readily allows us to reach temperatures of $\sim 85 \mu\text{K}$, with atom numbers of $\sim 10^8$ and phase-space densities of $\sim 5 \times 10^{-6}$ for both isotopes. When operating simultaneous cooling in which we cool ${}^7\text{Li}$ via the lower hyperfine state ($F_e = 1$) of the $2^2 P_{1/2}$ level, we find that the proximity of the ${}^7\text{Li}$ cooling light to the D_2 transition of ${}^6\text{Li}$ leads to the destruction of the ${}^6\text{Li}$ cloud. We resolved this issue by employing an alternating pulsed sequence of the cooling light, with which we were able to reach performances comparable to those above. In

conclusion, we have shown that ${}^6\text{Li}$ and ${}^7\text{Li}$ can be simultaneously laser cooled to temperatures $\lesssim 100 \mu\text{K}$, thus providing a significant simplification in the preparation of degenerate Bose-Fermi mixtures of these isotopes.

ACKNOWLEDGMENTS

We thank K. Dai, C. de Daniloff, S. Dhar, A. Hammond, J. Lis, S. Jin, J. Struck, and J. Verstraten for experimental assistance at various stages of this project. This work has been supported by Agence Nationale de la Recherche (Grant No. ANR-21-CE30-0021), the European Research Council (Grant No. ERC-2016-ADG-743159), CNRS (Tremplin@INP 2020), and Région Ile-de-France in the framework of DIM SIRTEQ (Super2D and SISCo).

-
- [1] C. Ospelkaus and S. Ospelkaus, *J. Phys. B* **41**, 203001 (2008).
 - [2] C. Chin, R. Grimm, P. Julienne, and E. Tiesinga, *Rev. Mod. Phys.* **82**, 1225 (2010).
 - [3] A. Schirotzek, C.-H. Wu, A. Sommer, and M. W. Zwierlein, *Phys. Rev. Lett.* **102**, 230402 (2009).
 - [4] N. Spethmann, F. Kindermann, S. John, C. Weber, D. Meschede, and A. Widera, *Phys. Rev. Lett.* **109**, 235301 (2012).
 - [5] M.-G. Hu, M. J. Van de Graaff, D. Kedar, J. P. Corson, E. A. Cornell, and D. S. Jin, *Phys. Rev. Lett.* **117**, 055301 (2016).
 - [6] N. B. Jørgensen, L. Wacker, K. T. Skalmstang, M. M. Parish, J. Levinsen, R. S. Christensen, G. M. Bruun, and J. J. Arlt, *Phys. Rev. Lett.* **117**, 055302 (2016).
 - [7] S. Laurent, M. Pierce, M. Delehaye, T. Yefsah, F. Chevy, and C. Salomon, *Phys. Rev. Lett.* **118**, 103403 (2017).
 - [8] R. S. Bloom, M.-G. Hu, T. D. Cumby, and D. S. Jin, *Phys. Rev. Lett.* **111**, 105301 (2013).
 - [9] R. Pires, J. Ulmanis, S. Häfner, M. Repp, A. Arias, E. D. Kuhnle, and M. Weidemüller, *Phys. Rev. Lett.* **112**, 250404 (2014).
 - [10] S.-K. Tung, K. Jiménez-García, J. Johansen, C. V. Parker, and C. Chin, *Phys. Rev. Lett.* **113**, 240402 (2014).
 - [11] K.-K. Ni, S. Ospelkaus, M. H. G. de Miranda, A. Pe'er, B. Neyenhuis, J. J. Zirbel, S. Kotochigova, P. S. Julienne, D. S. Jin, and J. Ye, *Science* **322**, 231 (2008).
 - [12] L. D. Carr, D. DeMille, R. V. Krems, and J. Ye, *New J. Phys.* **11**, 055049 (2009).
 - [13] P. K. Molony, P. D. Gregory, Z. Ji, B. Lu, M. P. Köppinger, C. R. Le Sueur, C. L. Blackley, J. M. Hutson, and S. L. Cornish, *Phys. Rev. Lett.* **113**, 255301 (2014).
 - [14] J. W. Park, S. A. Will, and M. W. Zwierlein, *Phys. Rev. Lett.* **114**, 205302 (2015).
 - [15] B. J. DeSalvo, K. Patel, J. Johansen, and C. Chin, *Phys. Rev. Lett.* **119**, 233401 (2017).
 - [16] R. S. Lous, I. Fritsche, M. Jag, B. Huang, and R. Grimm, *Phys. Rev. A* **95**, 053627 (2017).
 - [17] R. S. Lous, I. Fritsche, M. Jag, F. Lehmann, E. Kirilov, B. Huang, and R. Grimm, *Phys. Rev. Lett.* **120**, 243403 (2018).
 - [18] B. J. DeSalvo, K. Patel, G. Cai, and C. Chin, *Nature (London)* **568**, 61 (2019).
 - [19] I. Ferrier-Barbut, M. Delehaye, S. Laurent, A. T. Grier, M. Pierce, B. S. Rem, F. Chevy, and C. Salomon, *Science* **345**, 1035 (2014).
 - [20] X.-C. Yao, H.-Z. Chen, Y.-P. Wu, X.-P. Liu, X.-Q. Wang, X. Jiang, Y. Deng, Y.-A. Chen, and J.-W. Pan, *Phys. Rev. Lett.* **117**, 145301 (2016).
 - [21] R. Roy, A. Green, R. Bowler, and S. Gupta, *Phys. Rev. Lett.* **118**, 055301 (2017).
 - [22] R. Zhang, W. Zhang, H. Zhai, and P. Zhang, *Phys. Rev. A* **90**, 063614 (2014).
 - [23] T. Ozawa, A. Recati, M. Delehaye, F. Chevy, and S. Stringari, *Phys. Rev. A* **90**, 043608 (2014).
 - [24] Y. Castin, I. Ferrier-Barbut, and C. Salomon, *C. R. Phys.* **16**, 241 (2015).
 - [25] M. Abad, A. Recati, S. Stringari, and F. Chevy, *Eur. Phys. J. D* **69**, 126 (2015).
 - [26] Y. Jiang, R. Qi, Z.-Y. Shi, and H. Zhai, *Phys. Rev. Lett.* **118**, 080403 (2017).
 - [27] M. Delehaye, S. Laurent, I. Ferrier-Barbut, S. Jin, F. Chevy, and C. Salomon, *Phys. Rev. Lett.* **115**, 265303 (2015).
 - [28] A. T. Grier, I. Ferrier-Barbut, B. S. Rem, M. Delehaye, L. Khaykovich, F. Chevy, and C. Salomon, *Phys. Rev. A* **87**, 063411 (2013).
 - [29] A. Burchianti, G. Valtolina, J. A. Seman, E. Pace, M. De Pas, M. Inguscio, M. Zaccanti, and G. Roati, *Phys. Rev. A* **90**, 043408 (2014).
 - [30] G. Grynberg and J.-Y. Courtois, *Europhys. Lett.* **27**, 41 (1994).
 - [31] D. Boiron, C. Triché, D. R. Meacher, P. Verkerk, and G. Grynberg, *Phys. Rev. A* **52**, R3425 (1995).
 - [32] M. Weidemüller, T. Esslinger, M. A. Ol'shanii, A. Hemmerich, and T. W. Hänsch, *Europhys. Lett.* **27**, 109 (1994).
 - [33] F. Sievers, N. Kretzschmar, D. R. Fernandes, D. Suchet, M. Rabinovic, S. Wu, C. V. Parker, L. Khaykovich, C. Salomon, and F. Chevy, *Phys. Rev. A* **91**, 023426 (2015).
 - [34] D. S. Barker, E. B. Norrgard, N. N. Klimov, J. A. Fedchak, J. Scherschligt, and S. Eckel, *Opt. Express* **30**, 9959 (2022).

- [35] G. Colzi, G. Durastante, E. Fava, S. Serafini, G. Lamporesi, and G. Ferrari, *Phys. Rev. A* **93**, 023421 (2016).
- [36] D. Nath, R. K. Easwaran, G. Rajalakshmi, and C. S. Unnikrishnan, *Phys. Rev. A* **88**, 053407 (2013).
- [37] G. Salomon, L. Fouché, P. Wang, A. Aspect, P. Bouyer, and T. Bourdel, *Europhys. Lett.* **104**, 63002 (2013).
- [38] D. R. Fernandes, F. Sievers, N. Kretzschmar, S. Wu, C. Salomon, and F. Chevy, *Europhys. Lett.* **100**, 63001 (2012).
- [39] H.-Z. Chen, X.-C. Yao, Y.-P. Wu, X.-P. Liu, X.-Q. Wang, Y.-X. Wang, Y.-A. Chen, and J.-W. Pan, *Phys. Rev. A* **94**, 033408 (2016).
- [40] S. Rosi, A. Burchianti, S. Conclave, D. S. Naik, G. Roati, C. Fort, and F. Minardi, *Sci. Rep.* **8**, 1301 (2018).
- [41] C. J. Sansonetti, C. E. Simien, J. D. Gillaspay, J. N. Tan, S. M. Brewer, R. C. Brown, S. Wu, and J. V. Porto, *Phys. Rev. Lett.* **107**, 023001 (2011).
- [42] M.-O. Mewes, G. Ferrari, F. Schreck, A. Sinatra, and C. Salomon, *Phys. Rev. A* **61**, 011403(R) (1999).
- [43] B. Efron, *Ann Stat.* **7**, 1 (1979).
- [44] C. L. Satter, S. Tan, and K. Dieckmann, *Phys. Rev. A* **98**, 023422 (2018).
- [45] N. R. Hutzler, L. R. Liu, Y. Yu, and K.-K. Ni, *New J. Phys.* **19**, 023007 (2017).
- [46] A. Bergschneider, V. M. Klinkhamer, J. H. Becher, R. Klemt, G. Zürn, P. M. Preiss, and S. Jochim, *Phys. Rev. A* **97**, 063613 (2018).
- [47] P. D. Gregory, J. A. Blackmore, S. L. Bromley, and S. L. Cornish, *Phys. Rev. Lett.* **124**, 163402 (2020).
- [48] Y. Liu, M.-G. Hu, M. A. Nichols, D. D. Grimes, T. Karman, H. Guo, and K.-K. Ni, *Nat. Phys.* **16**, 1132 (2020).
- [49] M. A. Nichols, Y.-X. Liu, L. Zhu, M.-G. Hu, Y. Liu, and K.-K. Ni, *Phys. Rev. X* **12**, 011049 (2022).